Small

NANO · MICRO small
www.small-journal.com

RESEARCH ARTICLE

Tuning Pore Microenvironments in Covalent Organic Frameworks for Controlled Enzyme Loading and Release

Wenlu Fan[1] | Joshua Phipps[1] | Kui Tan[2] | Thamraa AlShahrani[3] | Shengqian Ma[1]

[1]Department of Chemistry, University of North Texas, Denton, USA | [2]Department of Chemistry and Biochemistry, University of Texas at El Paso, El Paso, USA | [3]Department of Physics, College of Science, Princess Nourah bint Abdulrahman University, Riyadh, Saudi Arabia

Correspondence: Shengqian Ma (shengqian.ma@unt.edu)

Received: 4 May 2026 | **Revised:** 12 July 2026 | **Accepted:** 22 July 2026

Keywords: controlled release | covalent organic framework | enzyme immobilization | papain | pore microenvironment

ABSTRACT

Covalent Organic Frameworks (COFs) with tunable pore environments provide a versatile platform for enzyme delivery; however, the relationship between pore microenvironment and enzyme loading and release behavior remains insufficiently explored. Herein, we report the synthesis of a series of TPE-based imine-linked COFs, constructed from tetrakis(4-aminophenyl)ethene (TPE-NH_2) and three dialdehyde linkers bearing different functional groups (—H, —CH_3, and N, S-containing heterocycles). These COFs exhibit distinct hydrophobic–hydrophilic characteristics while maintaining comparable structural backbones that allowed the selected COFs to act as models for the systematic investigation of their effect on papain loading, release, and activity. Furthermore, in situ FTIR spectroscopy directly probed the dynamic enzyme–framework interactions during loading, providing molecular-level evidence that supports the proposed role of the pore microenvironment in governing enzyme behavior. These results indicate that hydrophobic frameworks exhibit lower relative loading capacities, facilitate release, and partially compromise enzymatic activity for the model protein, whereas hydrophilic frameworks promote efficient loading, slow release, and lead to relatively lower retained activity. Together, this work provides molecular-level insights into how pore microenvironments regulate enzyme loading, release, and retained activity, establishing rational design principles for COF-based protein delivery and biocatalytic platforms.

1 | Introduction

The combination of enzymes and porous materials has been widely recognized as an effective strategy to regulate enzyme activity, stability, and reusability, thereby significantly enhancing their potential applicability in industrial biocatalysis, biotechnology, and protein delivery [1]. Among various host materials, covalent organic frameworks (COFs) have recently emerged as an attractive alternative to traditional supports due to their high crystallinity, structural regularity, and tunable pore architectures. Compared with other increasingly popular porous materials such as metal–organic frameworks (MOFs), COFs offer fully organic backbones and greater chemical design flexibility, enabling more precise modulation of pore size, topology, and surface functionality through rational monomer selection. Consequently, COFs have been extensively explored for enzyme immobilization. For example, by restricting enzyme conformational dynamics and mitigating leaching, confined systems can improve catalytic efficiency while reducing pathways of deactivation by denaturation or inhibition [2]. Further studies have also demonstrated their potential as enzyme loading–release platforms. This has been demonstrated by Chen et al. who developed COFs as crystalline sponges for enzyme capture, enrichment, and subsequent release [3].

All rights reserved, including rights for text and data mining and training of artificial intelligence technologies or similar technologies.
© 2026 Wiley-VCH GmbH

Papain, a cysteine protease derived from papaya latex, is an important model enzyme widely used in food processing, pharmaceuticals, and protein hydrolysis due to its high catalytic activity and broad substrate specificity [4]. As a globular protein with heterogeneous surface chemistry, papain contains both hydrophilic and hydrophobic domains, making it a good model candidate that is highly sensitive to its surrounding environment due to its many interactions with host materials [5–7]. In this scenario, excessively strong enzyme–framework interactions may hinder enzyme release and induce conformational restriction or partial denaturation, whereas overly weak interactions may result in insufficient loading or rapid enzyme leaching [8, 9]. Moreover, achieving a balance between high loading capacity and controlled release remains difficult as these two factors are often inversely correlated. Therefore, developing porous materials with finely tunable microenvironments that can regulate enzyme–host interactions is highly consequential for a range of applications and is of critical importance [10].

More contemporary studies have highlighted that enzyme performance within porous materials is strongly influenced by factors such as spatial arrangement, host–guest interactions, pore polarity and local physicochemical environments [11–14]. Rodrigues et al., for example, highlighted that pore polarity and hydrophilicity–hydrophobicity are key factors influencing protein adsorption, orientation, and stability within confined spaces [15]. Likewise, Fan et al. reported that the balancing of framework hydrophilicity and hydrophobicity was an important factor in enzyme immobilization [16]. However, whether a similar balance among pore polarity, hydrophilic–hydrophobic properties, and reversible enzyme–framework interactions governs enzyme loading, release, and retained activity in loading–release systems remains insufficiently explored. Moreover, systematic studies that isolate the influence of pore microenvironment while maintaining comparable framework topology and pore architecture also remain relatively limited, highlighting the need for further investigation to establish clear structure–microenvironment–property relationships for the rational design of COF-enzyme systems [17, 18].

With this in mind, we designed a series of TPE-based imine-linked COFs with systematically tunable pore microenvironments by employing structurally related dialdehyde linkers bearing distinct functional groups (—H, —CH_3, or N, S-containing heterocycles) [19, 20]. These molecular-design COFs enabled modulation of pore polarity and hydrophilicity–hydrophobicity without significantly altering the overall framework topology and were selected as a set of model candidates to investigate enzyme–framework interactions and evaluate how changes in the pore microenvironment and characteristics influence factors surrounding enzyme uptake, release, and retention of activity. The enzyme papain was chosen as a model enzyme for this study due to its size, shape, surface characteristics, and widespread application. By monitoring enzymatic activity quantitatively upon release using a colorimetric protease assay based on succinylated casein and trinitrobenzenesulfonic acid (TNBSA), the sensitive detection of proteolytic activity via the generation of primary amines was evaluated to draw conclusions on how the surrounding pore environment of the synthesized COFs influenced protein loading, release, and activity [21].

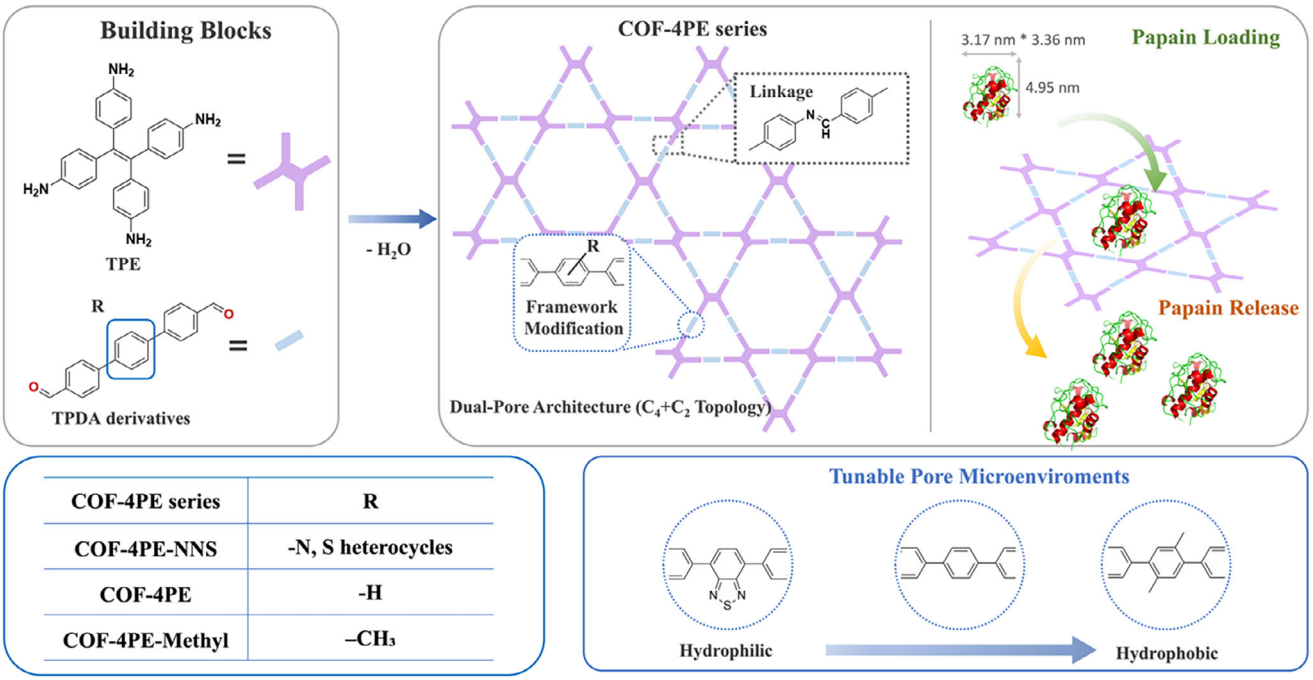
2 | Results and Discussion

2.1 | Materials Preparation and Physicochemical Characterization

Due to its well-defined architecture, we selected TPE-TPDA-COF (hereafter denoted as COF-4PE) with its C4 + C2 topology (Scheme 1), constructed via Schiff-base condensation between tetrakis(4-aminophenyl)ethene (TPE) and [1′:4′,1″-terphenyl]-4,4″-dicarboxaldehyde (TPDA) as a model framework. This COF represents a good candidate due to its large enzyme-accessible pores that closely match the dimensions of papain and can preserve a structurally analogous framework with systematically tunable pore chemistry that is sufficiently stable under the experimental conditions employed in this study. Such a platform enables the investigation of reversible enzyme–framework interactions in loading–release systems without introducing significant variations in framework topology. By introducing TPDA derivatives bearing different substituents (R═H, —CH_3, and N, S-containing heterocycles) to work as framework modifications at the pore interface, a series of COF-4PE materials with systematically varied pore microenvironments were obtained without significantly altering the overall framework topology. This experimental design enables a direct comparison of how pore microenvironment factors such as hydrophilicity–hydrophobicity influence enzyme loading and release behavior within structurally comparable porous frameworks.

To evaluate enzyme loading, the as-synthesized COFs were incubated with a papain solution at 4°C for 3 days. The resulting solids were subsequently washed twice with acetonitrile to remove loosely adsorbed papain species from the external surface, affording composites denoted as papain@COFs. The loading capacity of papain was determined using UV–vis spectroscopy by measuring the concentration difference between the initial papain solution and the combined supernatant and washing solutions after the loading process. To determine release, papain@COFs were dispersed in PBS buffer and subjected to gentle inversion to facilitate enzyme release. The suspension was then filtered, and the collected filtrate was analyzed by UV–vis spectroscopy and enzymatic activity assays to evaluate the release efficiency and the retained activity of the released papain. (See the details in the experimental section of the Supporting Information.)

To confirm the loading of our model enzyme, we performed FTIR analysis of COF-4PE before, after loading, and following release (Figure 1a). These results indicate that the pristine COF-4PE exhibits a characteristic imine (C═N) stretching band at ~1620 cm^{-1}, which is retained after loading, demonstrating the preservation of the COF structure. In Papain@COF-4PE, we observed enhanced bands at ~1650 and ~1548 cm^{-1}, which can be assigned to the amide I and amide II vibrations of papain, respectively, thereby verifying enzyme incorporation [1]. Additionally, the band at ~1700 cm^{-1} in the pristine COF-4PE was attributed to residual aldehyde (C═O) groups. This peak disappeared after loading, which can be ascribed to interactions with the amino residues of papain, possibly involving imine formation or strong hydrogen bonding [27]. The spectra of Papain@COF-4PE after release retain the characteristic papain bands at ~1650 cm^{-1} (amide I) and ~1546 cm^{-1} (amide II), indicating that a small



SCHEME 1 | Schematic illustration of the synthetic route of the COF-4PE series and papain loading and release process.

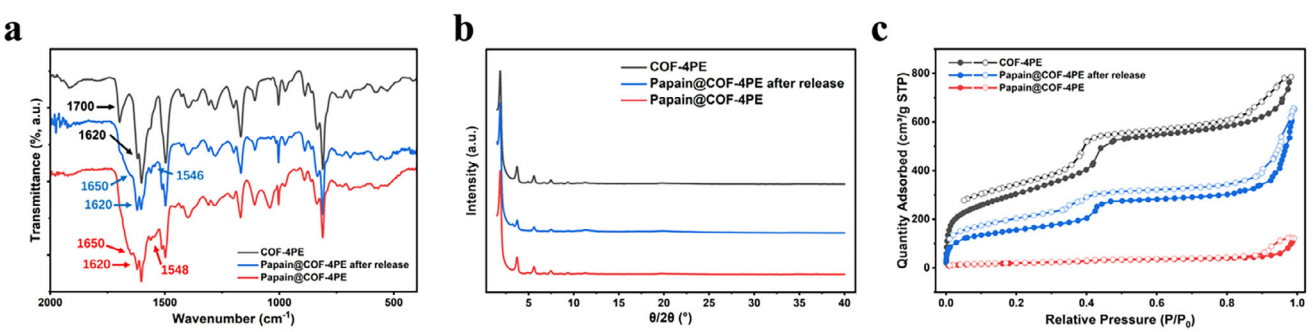
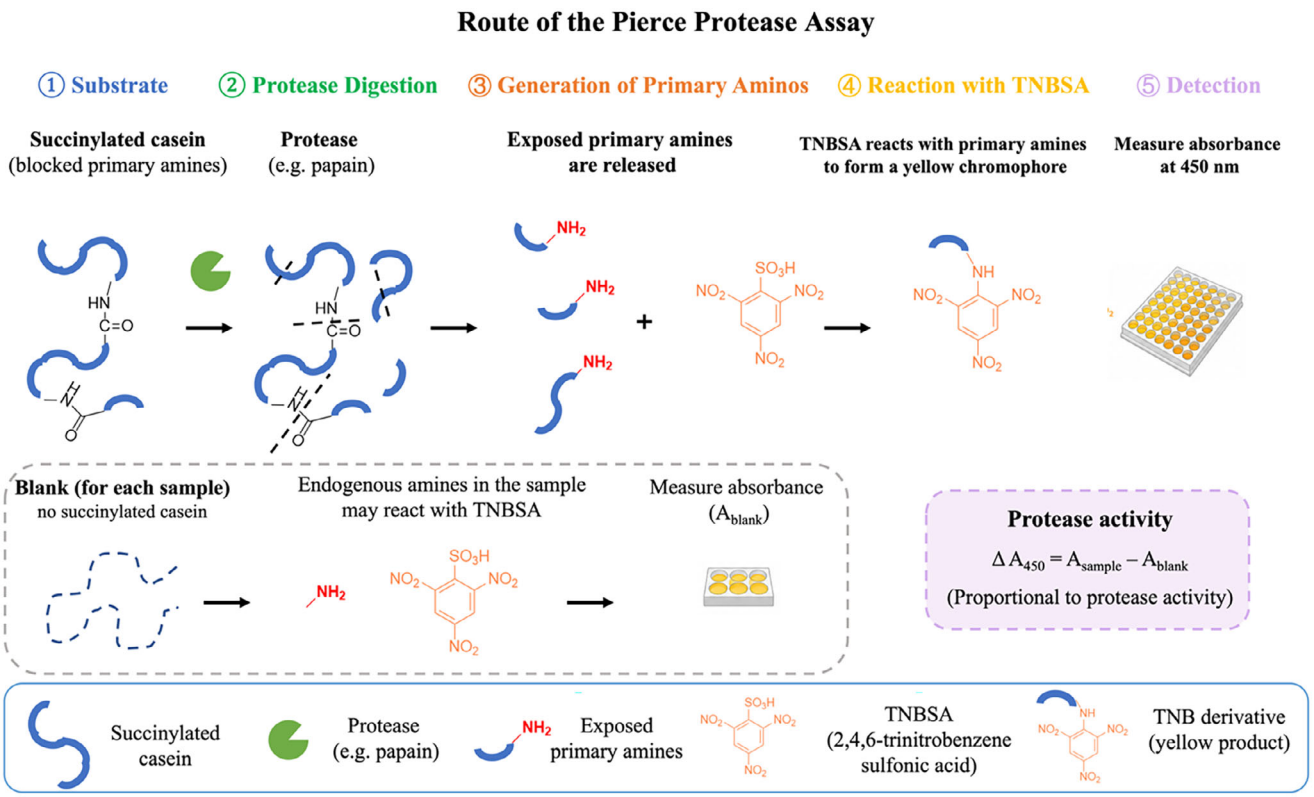


FIGURE 1 | Characterization of COFs: (a) FT-IR spectra of COF-4PE (black), Papain@COF-4PE after release (blue), and Papain@COF-4PE (red). (b) PXRD patterns of COF-4PE (black), Papain@COF-4PE after release (blue), and Papain@COF-4PE (red). (c) The N_2 adsorption isotherms of COF-4PE (black), Papain@COF-4PE after release (blue), and Papain@COF-4PE (red).

amount of papain remains within the COF framework. However, when normalized to the aromatic C—H out-of-plane deformation peak at 810 cm^{-1}, the relative intensities of the amide I and amide II decreased after release, indicating that a substantial fraction of the loaded papain had dissociated from the framework.

To evaluate the retention of the COF structure throughout the experiment, we performed Powder X-ray diffraction (PXRD) analysis of a representative sample from each COF group, including before loading, after loading, and following protein release (Figure 1b). From this, we observed that the patterns of Papain@COF-4PE (red) and Papain@COF-4PE after release (blue) exhibit diffraction peaks at similar 2θ positions to those of pristine COF-4PE (black), thus indicating that the long-range ordered framework remains intact throughout the experiment. Following PXRD, nitrogen sorption isotherms were measured at 77 K for each sample group (Figure 1c). The pore size distribution derived from density functional theory analysis showed that COF-4PE exhibits two distinct pore sizes centered at 3.7 and 1.3 nm (Table S1), corresponding to its dual-pore architecture [20]. Furthermore, the Brunauer–Emmett–Teller (BET) surface area of COF-4PE decreased significantly from 1091 to 60 $m^2\ g^{-1}$ after papain loading, and subsequently recoverd to 457 $m^2\ g^{-1}$ following papain release, confirming successful papain accommodation within the COF pores and the subsequent release of a substantial fraction of the loaded enzyme. While both COF-4PE (black) and Papain@COF-4PE after release (blue) exhibited a typical type IV behavior with a distinct hysteresis loop indicative of a mesoporous structure with well-defined pore channels, the Papain@COF-4PE (red) lacked this shape and instead was flattened, supporting the successful inclusion of papain within the COF pores. The recovery of the COF pores after release of loaded guest molecules also complements the PXRD, indicating that the structure of the COF is retained and that the pores remain



SCHEME 2 | Illustration showing the progression of a colorimetric protease assay based on succinylated casein and trinitrobenzenesulfonic acid (TNBSA).

accessible. Likewise, COF-4PE-NNS and COF-4PE-Methyl exhibited structural and surface area properties similar to those of COF-4PE, with only slight differences, as shown in Figures S3 and S4 and Table S1.

2.2 | Effect of Pore Microenvironment on Molecular Loading and Release

The proteolytic activity of papain was evaluated using a colorimetric assay with succinylated casein as the substrate. Upon enzymatic hydrolysis, papain cleaves peptide bonds in succinylated casein, generating primary amine groups that subsequently react with TNBSA to produce a chromogenic product detectable at 450 nm (Scheme 2) [22]. The observed increase in absorbance is directly proportional to the protease activity and reflects the extent of substrate degradation. Leveraging this method, the activity of the enzyme was determined both within a standard COF host (COF-4PE) and after release under standard (borate buffer, pH 8.5, 4 °C) and experimental conditions. The results of these tests are described in greater detail below.

2.2.1 | Loading and Release Conditions

2.2.1.1 | Effect of Buffer. To evaluate how buffer characteristics influenced enzyme loading, release, and activity, we selected 3 buffers compatible with papain stability: Borate, Tris-HCl, and HEPES, each at pH 8.5. For each of these, we observed loading capacities after 24 h (mg enzyme•mg COF^{-1}) of 0.43, 0.50, and 0.47, respectively (Figure 2a). While there was little variance, Tris-HCl attained the highest loading during this period, suggesting that in this buffer environment, papain adsorption is promoted within the COF framework, likely through enhanced hydrogen bonding and electrostatic interactions. To monitor release, we used a standard solution of PBS buffer (50 mM, pH 7.4) to compare each trial. Here, Tris-HCl showed the greatest retention of the enzyme, with the proportion of released enzyme being 18.0% compared to 30.7% for the Borate buffer and 22.6% for the HEPES (Figure 3a). This lower proportion of released enzyme for Tris-HCl again indicates a stronger guest-host interaction, with less of the enzyme being allowed to leave the COF pore. To compare the effectiveness of the buffer to promote enzyme stability and activity after delivery, we then evaluated the activity of the papain released from the framework. This is reported here as a proportion of activity (mg of active enzyme/mg of released papain), with Tris-HCl attaining 82.6%, Borate 89%, and HEPES 74.0% (Figure 4a). These results suggest that there is a greater affinity between the enzymes and the COF in the presence of Tris-HCl compared to the other buffers, leading to a weaker stabilization of the functional form of the enzyme that is reflected in the activity of the released Papain.

2.2.1.2 | Loading Temperature. To optimize the enzyme loading conditions, papain was loaded onto the COFs at 4°C and at room temperature (21°C), two representative temperatures we selected as they are routinely used for protein adsorption experiments. This comparison was designed to evaluate the balance between enzyme structural preservation and loading efficiency under practically relevant conditions. After 1 day of

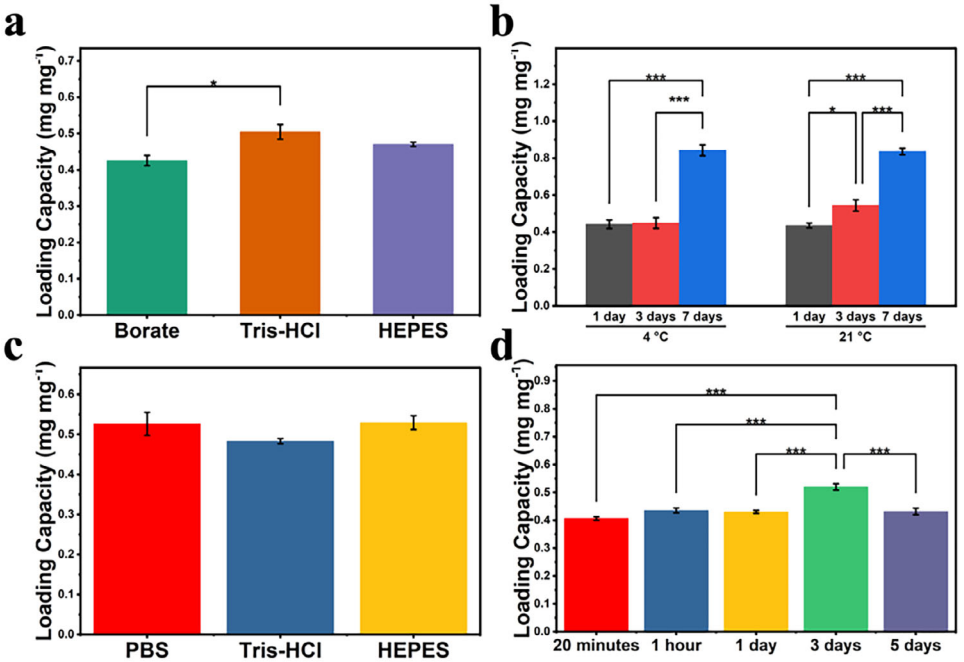


FIGURE 2 | The Loading Capacity (mg enzyme•mg^{-1} COF) of COF-4PE incubated with papain solution (10 mg mL^{-1}). (a) Loading at 4°C with varied buffer solution (borate buffer, Tris-HCl, HEPES buffer) for 1 day and released in PBS buffer solution at R. T., (b) loading at varied temperature (4°C and R. T.) with borate buffer solution for 1, 3, and 7 days and release in PBS buffer solution at R. T., (c) loading at 4°C with borate buffer solution for 3 days and then release in varied buffer solution (PBS, Tris-HCl, HEPES) at R. T., and (d) loading at 4°C with borate buffer solution for 20 min, 1 h, 1 day, 3 days, and 5 days followed by release in PBS buffer solution at R. T. (* $p \leq 0.05$, ** $p \leq 0.01$, *** $p \leq 0.001$).

incubation, the loading capacities at 4°C (0.44 mg mg^{-1}) and room temperature (21°C, 0.43 mg mg^{-1}) were nearly identical (Figure 2b). After 3 days, a moderately higher loading capacity was observed at room temperature (0.54 mg mg^{-1}) compared to loading at 4°C (0.45 mg mg^{-1}). This is likely due to enhanced molecular diffusion at the higher temperature, which facilitates papain access within the interior of the COF, allowing for interaction with a greater number of adsorption sites within the COF frameworks. In addition, the increased thermal energy allows weaker guest–host interactions to be disrupted more readily, providing greater molecular mobility and enabling faster redistribution of papain within the pore network. However, after 7 days, the loading capacity at both temperatures reached the same loading capacity (0.84 mg mg^{-1}), indicating that temperature primarily influences the kinetics of enzyme loading rather than the ultimate loading capacity. When we compared the activity of the released enzymes between the two groups, we observed that the papain loaded at 4°C exhibited higher activity retention, indicating that lower temperatures better preserve the native conformation of the enzyme during loading (Figure 4b). These results suggest that, although room temperature somewhat favors mass transfer, mild low-temperature conditions mitigate thermal and conformational stress and suppress excessive interfacial interactions between papain and the COF surface.

2.2.1.3 | Release Buffer. Next, we further investigated how the selection of buffer effects on enzyme release and retention of activity. As shown in Figure 3c, using PBS during release resulted in a slightly higher release percentage (31.2%) compared to Tris-HCl (27.4%) and HEPES (23.9%). This is likely due to its ionic strength, which weakens electrostatic interactions and hydrogen bonding between papain and the COF-4PE framework, facilitating mobility and a greater influence by diffusive forces encouraging release. In contrast, HEPES and Tris-HCl led to lower release but a higher retention of activity, 83.9% and 80.0%, respectively, compared to PBS, which attained 54.6% (Figure 4c). These results suggest that HEPES and Tris-HCl provide milder microenvironments that better preserve the native structure of papain during the release process.

2.2.1.4 | Loading Time. We then turned to examining the influence that loading duration exerts on the amount of enzyme loaded. Here, we observed a pronounced effect on loading capacity, release behavior, and retained activity. As shown in Figure 2d, the loading capacity increased with time and reached a maximum at 3 days (0.51 mg•mg^{-1}). After this period, we observed a decrease in loading at 5 days (0.43 mg•mg^{-1}). This behavior is consistent with a previous report where Phipps et al. observed a rebound effect while loading an enzyme within another framework (ADH in PCN-333) and is likely the result of overcrowding and concentration gradients [23–25]. These results support that assertion and indicate that papain uptake involves not only the same rapid adsorption but also slower diffusion into the COF pores until crowding overcomes the concentration gradient and diffusion leads to a decrease in loading. When we examined how this extended loading influenced release or activity, we observed a similar trend where the increased loading led to a smaller amount of released enzyme, but higher relative activity (Figures 3d and 4d). This prolonged contact and saturation of hydrophilic groups likely strengthened papain–COF interactions, leading to greater confinement and reduced release efficiency. Additionally, the activity profile suggests that this increased loading is not

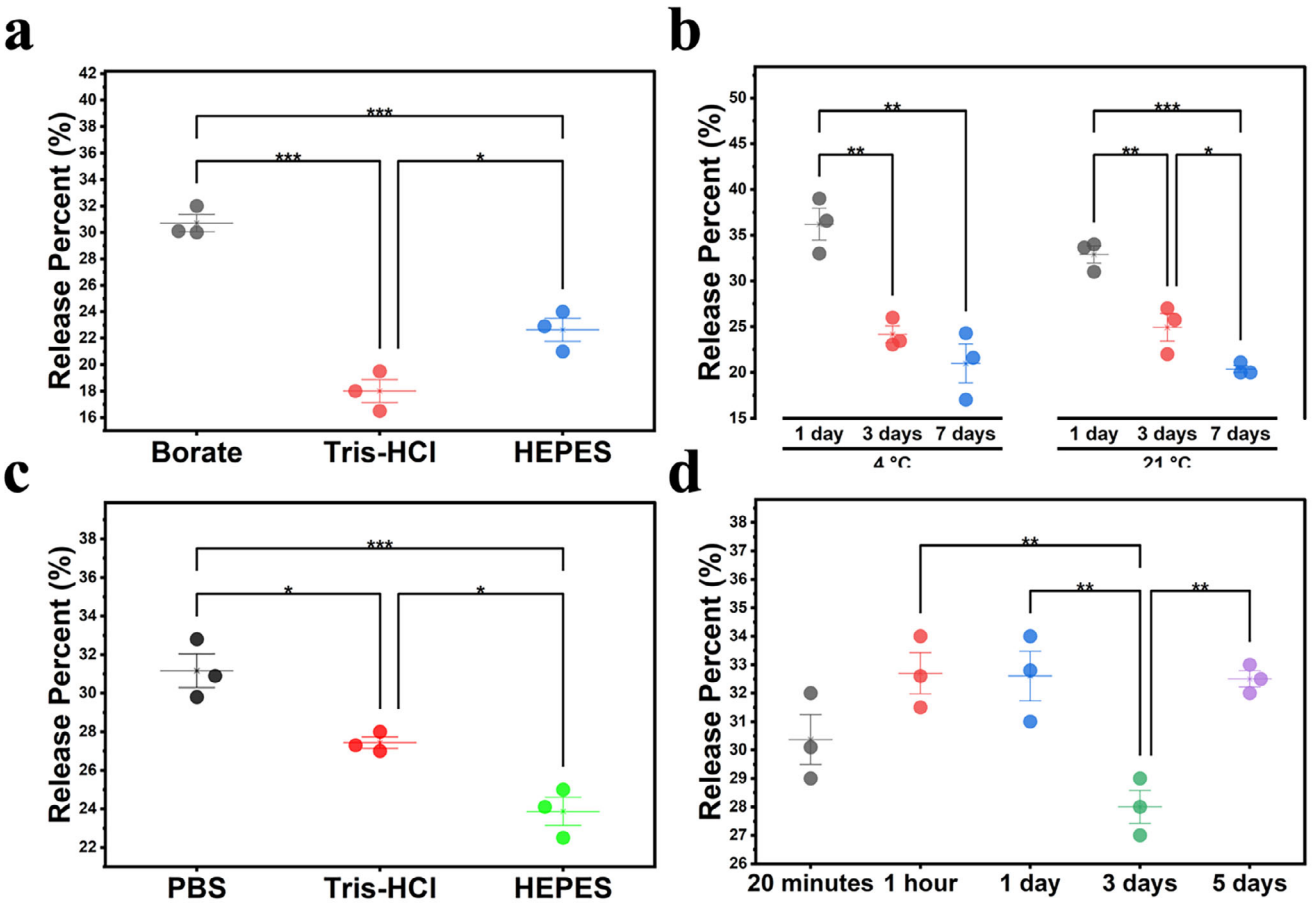


FIGURE 3 | The release percent (%) of COF-4PE incubation with papain solution (10 mg mL^{-1}) (a) Loading at 4°C with varied buffer solution (borate buffer, Tris-HCl, HEPES buffer) for 1 day and released in PBS buffer solution at R. T., (b) loading at varied temperature (4°C and R. T.) with borate buffer solution for 1, 3, and 7 days and release in PBS buffer solution at R. T., (c) loading at 4°C with borate buffer solution for 3 days and then release in varied buffer solution (PBS, Tris-HCl, HEPES) at R. T., and (d) loading at 4°C with borate buffer solution for 20 min, 1 h, 1 day, 3 days, and 5 days followed by release in PBS buffer solution at R. T. (* $p \leq 0.05$, ** $p \leq 0.01$, *** $p \leq 0.001$).

conducive to enzyme release; therefore, the optimal loading time when considering enzyme delivery will be at point with moderate confinement.

2.2.2 | The Role of Functional Groups

2.2.2.1 | Effect of Functionalization on Loading. To investigate the effect that functional groups have on loading capacity and release, we synthesized a variety of COF-4PE variants to evaluate alongside our pristine (hydrogen-functionalized) COF. These included functionalization with N, S-containing heterocycles (hereafter denoted as NNS) and methyl functional groups. We then evaluated the loading of enzyme into each of these COFs, where significant differences were observed, with the NNS group achieving the highest loading of 0.56 mg•mg^{-1}, followed by the pristine COF (0.51 mg•mg^{-1}) and the methyl COF (0.43 mg•mg^{-1}) (Figure 5a). We then measured contact angles, which revealed angles of 72.8°, 62.1°, and 88.9° for COF-4PE, COF-4PE-NNS, and COF-4PE-Methyl, respectively, confirming that the addition of different functional groups effectively modulated the pore microenvironment and produced the expected hydrophilicity/hydrophobicity and wettability trends.

As shown in Figure S6, subtraction of the water contribution from the FTIR spectrum of the papain solution revealed a pronounced C—O stretching (ν) band at 1044 cm^{-1}, originating from the hydroxyl-containing side chains of Ser, Thr, and Tyr residues. Compared with solid papain, where extensive hydrogen-bonding networks are present to hold the structure [26], this band exhibited a blue shift from 1029 to 1044 cm^{-1} (Figure 6a, top), indicating that papain adopts a distinct conformation through weaker hydrogen-bonding with surrounding water molecules in aqueous solution. A similar spectral evolution was observed during the papain loading process. Difference spectra referenced to the H_2O-submerged COF-4PE sample (Figure 6a, middle) showed a gradual shift of the C—O band from 1044 to 1039 cm^{-1}, implying the immobilization of papain from the aqueous phase into the solid COF pores. This result further suggests that the COF provides a microenvironment resembling that of bulk water yet exhibiting stronger H-bonding interactions that serve as driving forces for papain immobilization.

The initial difference spectra (Figure 6b, top) indicate that both COF-4PE-NNS and COF-4PE-Methyl provide a loading environment similar to that of COF-4PE. However, the interaction between water and COF-4PE-NNS is substantially stronger, which assists in the adsorption of papain. In particular, the

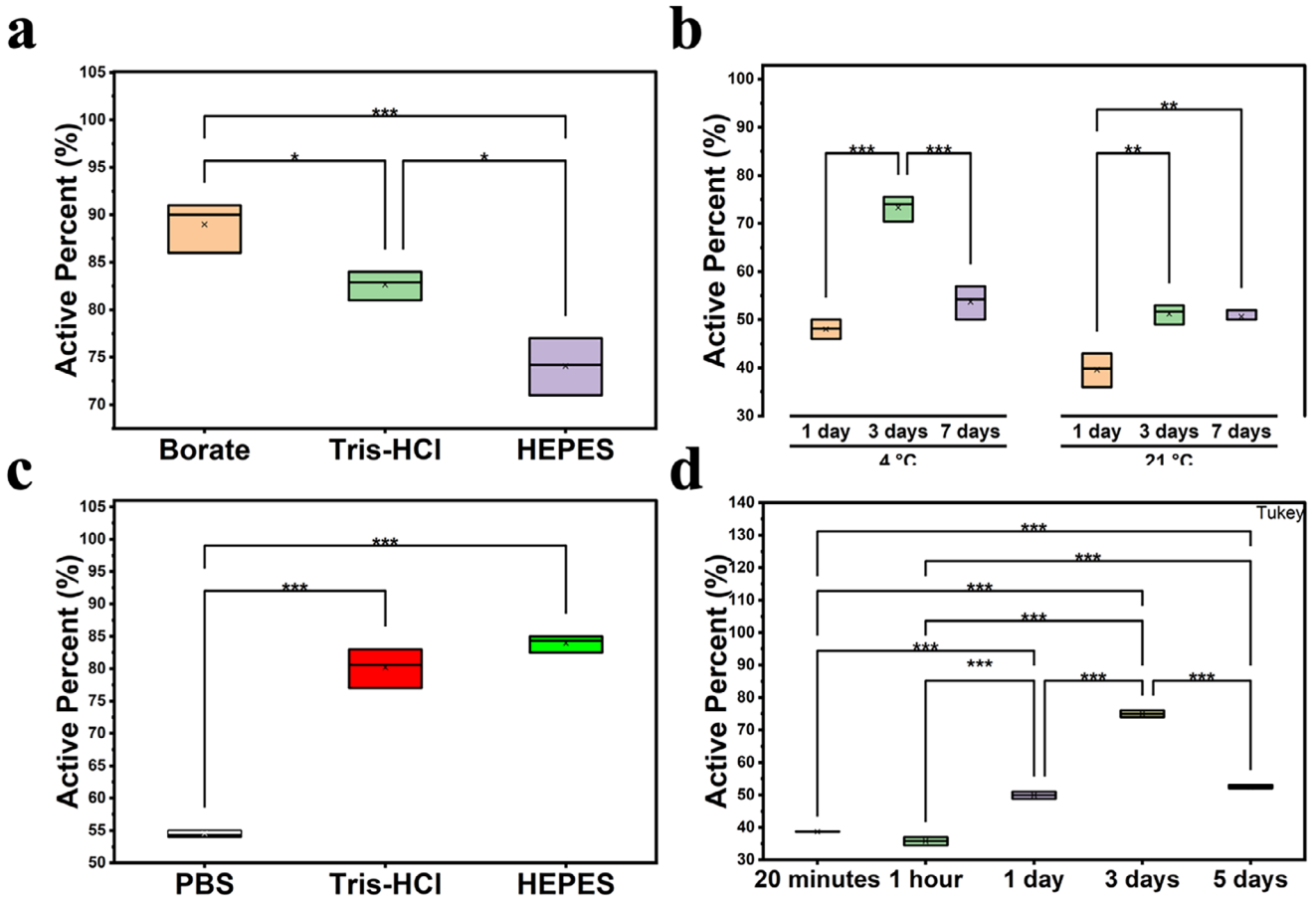


FIGURE 4 | The active percent (%) of COF-4PE incubated with papain solution (10 mg mL^{-1}). (a) Loading at 4°C with varied buffer solution (borate buffer, Tris-HCl, HEPES buffer) for 1 day and released in PBS buffer solution at R. T., (b) loading at varied temperature (4°C and R. T.) with borate buffer solution for 1, 3, and 7 days and release in PBS buffer solution at R. T., (c) loading at 4°C with borate buffer solution for 3 days and then release in varied buffer solution (PBS, Tris-HCl, HEPES) at R. T., and (d) loading at 4°C with borate buffer solution for 20 min, 1 h, 1 day, 3 days, and 5 days followed by release in PBS buffer solution at R. T. (* $p \leq 0.05$, ** $p \leq 0.01$, *** $p \leq 0.001$)

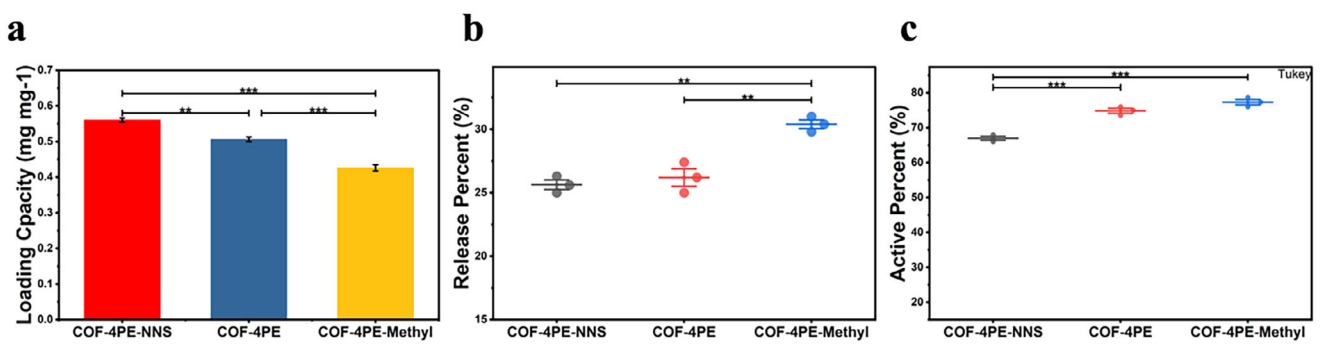


FIGURE 5 | (a) The loading capacity, (b) the release percentage, and (c) the active percent of various COFs materials (COF-4PE-NNS, COF-4PE, and COF-4PE-Methyl) with the incubation of papain solution (10 mg mL^{-1}) in borate buffer at 4°C for 3 days and release in PBS buffer solution. (* $p \leq 0.05$, ** $p \leq 0.01$, *** $p \leq 0.001$).

pronounced growth of the O—H stretching broad band at 3050–3550 cm^{-1}, mainly associated with hydrogen-bonded water molecules, demonstrates that water molecules actively participate in the loading process of papain in the relatively more hydrophilic COF-4PE-NNS. This is consistent with its higher papain loading capacity. As shown in Figure 6b bottom, after normalization to the intensity of the 1039 cm^{-1} band of papain, COF-4PE-NNS (black line) exhibited a stronger increase in both the 1652 cm^{-1} amide I (C═O stretching) band and the 3050–3550 cm^{-1} O—H broad band, suggesting that multiple hydrogen-bonding sites within the COF structure facilitate papain immobilization. Another contrasting point is found in COF-4PE-Methyl (green

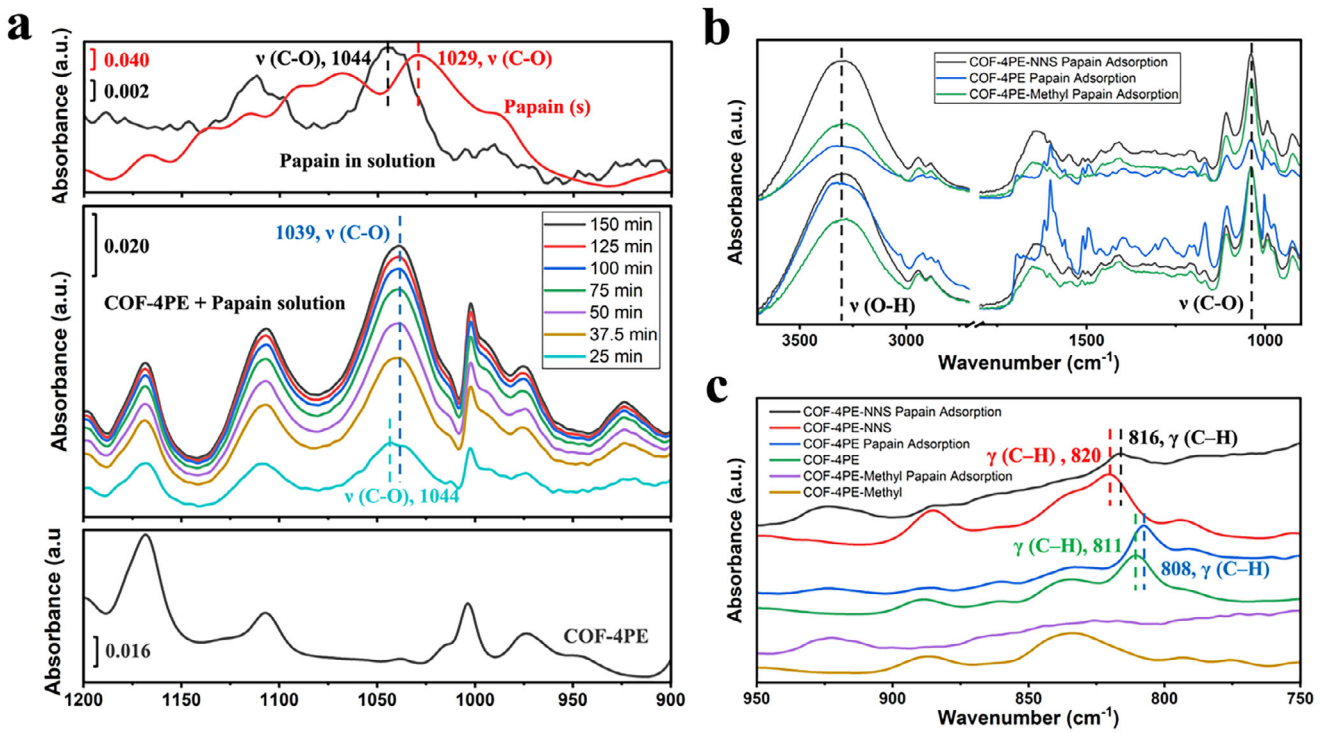


FIGURE 6 | (a) Top: IR spectra of papain solid (red) and papain in solution (black). Middle: difference spectra of submersing COF-4PE in papain solution for 25 min. (cyan), 37.5 min. (yellow), 50 min. (purple), 75 min. (green), 100 min. (blue), 125 min. (red), and 150 min. (black) referenced to the H_2O-submersion COF-4PE sample. Bottom: IR spectra of COF-4PE. (b) Difference spectra of submersing COF-4PE-NNS (black), COF-4PE (blue), and COF-4PE-Methyl (green) in papain solution for 150 min. Referenced to the respective H_2O-submersion COF sample. (The top 3 lines represent the original difference spectra, whereas the bottom 3 lines represent the difference spectra normalized via the intensity of the 1039 cm^{-1} peak in the black line as the reference). (c) IR spectra of submersing COF-4PE-NNS in papain solution for 150 min. (black), COF-4PE-NNS (red), submersing COF-4PE in papain solution for 150 min. (blue), COF-4PE (green), submersing COF-4PE-Methyl in papain solution for 150 min. (purple), and COF-4PE-Methyl (yellow). The black, blue, and purple lines were presented as the differential spectra to show the sequential changes occurring during papain adsorption. (Difference spectra referenced to the respective H_2O-submersion of each COF sample.) Notations and acronyms: ν, stretch; γ, deformation.

line), which primarily interacts with the hydroxyl-containing side chains of Ser, Thr, and Tyr residues along with other relatively weaker interactions, consistent with its lowest loading capacity. The influence of pore microenvironment functionalization in the COF framework on the papain loading process was further reflected by IR spectra changes in the aromatic C—H out-of-plane deformation (γ) peaks (Figure 6c) [27, 28]. Upon papain adsorption, the characteristic aromatic γ (C—H) peak exhibited red shifts from 820 to 816 cm^{-1} for COF-4PE-NNS and from 811 to 808 cm^{-1} for COF-4PE, indicating COF framework–protein interactions. Conversely, COF-4PE-Methyl showed little spectral perturbation, suggesting that its more hydrophobic pore environment disfavors papain interaction and binding.

Overall, these results indicate that the nature of the functional groups on the linker plays a decisive role in tuning the pore microenvironment and consequently the loading behavior of papain. The phenyl group in the pristine COF, with multiple relatively limited interaction sites, provides a moderately hydrophobic environment, resulting in moderate loading capacity [29]. In contrast, the introduction of N, S-containing heterocycles significantly enhances the hydrophilicity and introduces potential hydrogen-bonding and dipole interaction sites, thereby strengthening enzyme–COF framework interactions and leading to higher loading capacity [30]. Finally, the presence of methyl groups (—CH_3) creates a relatively more hydrophobic environment, promoting enzyme adsorption through hydrophobic interactions but offering limited specific binding sites or interactions, resulting in the lowest loading [31, 32]. Together, these results indicate that papain loading is governed by a balance between pore polarity, hydrophobicity, and accessible interaction sites. Functional groups that provide moderate hydrophilicity and multiple interaction modes (e.g., hydrogen bonding and dipole interactions) while maintaining pore accessibility are more favorable for enzyme uptake, whereas weak interactions limit loading efficiency and more hydrophobic groups lead to improved protein mobility and release.

2.2.2.2 | Effect of Functionalization on Release and Activity. Next, we examined the effect that these functional groups had on the release and the retention of enzyme activity. As shown in Figure 5b, the corresponding release profiles of these COFs showed an inverse trend compared to loading capacity, with the NNS-functionalized COF releasing the lowest amount at 25.6%, followed by the pristine COF and the methyl-functionalized COF at 26.2% and 34.0%, respectively. We then

observed another inverse trend where increasing hydrophilicity of functional groups led to lower retention of enzyme activity. Here, the methyl-functionalized COF showed 77.3% retained activity, followed by the pristine COF at 74.8% and the NNS-functionalized COF at 67.0% (Figure 5c). These results indicate that the release and the retained enzymatic activity of papain after release are strongly dependent on the pore microenvironment defined by the presence of different functional groups [29]. The COF bearing N, S-containing heterocycles exhibited relatively lower release percent and lower activity retention, despite its higher loading capacity, suggesting that the strong enzyme–framework interactions and tighter confinement may induce conformational restrictions or partial denaturation of papain. In contrast, the papain in the presence of the methyl-functionalized COF exhibited comparatively higher release percent and higher activity retention, indicating the presence of a weaker but more balanced relationship between interaction strength and pore environment, which better promoted release and preserved the native conformation of the enzyme.

Overall, these results indicate a few key findings. Functional groups that introduce strong interactions (e.g., NNS heterocycles) enhance enzyme loading by promoting hydrogen bonding, dipole–dipole, and hydrophobic interactions, but simultaneously hinder release and reduce activity, likely due to excessive confinement and/or conformational restriction. In contrast, other relatively weak interactions (e.g., CH_3) lead to reduced loading but facilitate enzyme release and retain greater enzyme activity. Together, these results show that enzyme performance in COF systems is dictated by a delicate balance between interaction strength, pore accessibility, and microenvironment compatibility. Building upon this foundation will allow for rational tuning of these factors, enabling simultaneous optimization of loading, release, and activity, thus providing important design principles for advanced COF-based enzyme immobilization and delivery systems.

3 | Conclusion

In this work, we established a controllable platform based on TPE-derived COFs to elucidate how pore microenvironments govern enzyme behaviors including loading, stability, and release. By systematically varying linker functional groups, we demonstrated that the polarity, hydrophilicity–hydrophobicity, and interaction modes within the pores could be finely tuned without altering the overall framework topology. Using papain as a model enzyme, we were able to reveal that enzyme performance is dictated by a relationship between interaction strength and microenvironment compatibility, where strong, multi-point interactions favor high uptake but lead to reduced activity, while weaker interactions facilitate mobility and release at the expense of loading. These findings reveal that precise regulation and balance of pore microenvironments, rather than structural parameters alone, can be key to optimizing enzyme–COF systems and provide actionable design principles for advanced porous platforms in biocatalysis and protein delivery. Together, this work provides a strong base of evidence that can be leveraged by our field to expand and improve the storage and delivery of proteinaceous species such as enzymes for enhanced uptake and controlled release.

Author Contributions

Joshua Phipps: writing – review and editing, methodology. **Thamraa Alshahrani**: funding acquisition, resources. **Wenlu Fan**: methodology, data curation, investigation, validation, formal analysis, writing – original draft. **Shengqian Ma**: conceptualization, funding acquisition, supervision, writing – review and editing. **Kui Tan**: investigation, data curation, formal analysis.

Acknowledgements

This work was supported by the Robert A. Welch Foundation (B-0027) (S.M.). Partial support from Princess Nourah Bint Abdulrahman University Researchers Supporting Project (PNURSP2026R1), Riyadh, Saudi Arabia is also acknowledged (T.A.). The in situ IR spectroscopy studies were supported by NSF award No. 2530186 (K. T. and S. M.).

Funding

This work was supported by the Robert A. Welch Foundation (B-0027) and Princess Nourah Bint Abdulrahman University Researchers Supporting Project (PNURSP2026R1).

Conflicts of Interest

The authors declare no conflicts of interest.

Data Availability Statement

The data that support the findings of this study are available from the corresponding author upon reasonable request.

References

1. Q. Sun, C. W. Fu, B. Aguila, et al., "Pore Environment Control and Enhanced Performance of Enzymes Infiltrated in Covalent Organic Frameworks," *Journal of the American Chemical Society* 140, no. 3 (2018): 984–992, https://doi.org/10.1021/jacs.7b10642.

2. Q. Sun, Y. Pan, X. Wang, et al., "Mapping Out the Degree of Freedom of Hosted Enzymes in Confined Spatial Environments," *Chemistry* 5, no. 12 (2019): 3184–3195, https://doi.org/10.1016/j.chempr.2019.10.002.

3. S. Paul, M. Gupta, S. Karak, et al., "Coprecipitated Enzyme-Encapsulated Covalent Organic Frameworks for Biocatalysis," *Journal of the American Chemical Society* 147, no. 27 (2025): 23724–23732, https://doi.org/10.1021/jacs.5c05496.

4. V. G. Tacias-Pascacio, R. Morellon-Sterling, D. Castañeda-Valbuena, et al., "Immobilization of Papain: A Review," *International Journal of Biological Macromolecules* 188 (2021): 94–113, https://doi.org/10.1016/j.ijbiomac.2021.08.016.

5. X. Wang, L. He, J. Sumner, et al., "Spatially Confined Protein Assembly in Hierarchical Mesoporous Metal-Organic Framework," *Nature Communications* 14, no. 1 (2023): 973, https://doi.org/10.1038/s41467-023-36533-w.

6. R. A. Sheldon and S. van Pelt, "Enzyme Immobilisation in Biocatalysis: Why, What and How," *Chemical Society Reviews* 42, no. 15 (2013): 6223–6235, https://doi.org/10.1039/C3CS60075K.

7. M. Hartmann and X. Kostrov, "Immobilization of Enzymes on Porous Silicas—Benefits and Challenges," *Chemical Society Reviews* 42, no. 15 (2013): 6277, https://doi.org/10.1039/C3CS60021A.

8. X. Wang, P. C. Lan, and S. Ma, "Metal–Organic Frameworks for Enzyme Immobilization: Beyond Host Matrix Materials," *ACS Central Science* 6, no. 9 (2020): 1497–1506, https://doi.org/10.1021/acscentsci.0c00687.

9. W. Liang, H. Xu, F. Carraro, et al., "Enhanced Activity of Enzymes Encapsulated in Hydrophilic Metal–Organic Frameworks," *Journal of the American Chemical Society* 141, no. 6 (2019): 2348–2355, https://doi.org/10.1021/jacs.8b10302.

10. X. Wang, L. He, J. Sumner, et al., "Spatially Confined Protein Assembly in Hierarchical Mesoporous Metal-organic Framework," *Nature Communications* 14, no. 1 (2023): 973, https://doi.org/10.1038/s41467-023-36533-w.

11. S. Qiao, Y. Sun, K. Wang, et al., "Dynamic Exchange Assembly of Enzymes With Single-Crystal Covalent Organic Frameworks," *Journal of the American Chemical Society* 148, no. 9 (2026): 9892–9900, https://doi.org/10.1021/jacs.5c22300.

12. X. Wang, L. He, S. Qian, S. Su, O. K. Farha, and S. Ma, "Monitoring Enzyme Clustering in a Highly Crystalline Metal–Organic Framework by Small-Angle Neutron Scattering," *Angewandte Chemie International Edition* 65, no. 4 (2026): 22967, https://doi.org/10.1002/anie.202522967.

13. J. Han, Z. Xing, Q. Guo, et al., "Covalent Organic Framework Nanosheets for the Assembly of Efficient Membrane Bioreactors," *Angewandte Chemie International Edition* 64, no. 28 (2025): 202505797, https://doi.org/10.1002/anie.202505797.

14. H. Chen, C. Jin, X. Chen, et al., "Covalent Organic Frameworks as Crystalline Sponges for Enzyme Extraction and Production From Natural Biosystems," *Chemical Engineering Journal* 444 (2022): 136624, https://doi.org/10.1016/j.cej.2022.136624.

15. R. C. Rodrigues, J. J. Virgen-Ortíz, J. C. S. dos Santos, et al., "Immobilization of Lipases on Hydrophobic Supports: Immobilization Mechanism, Advantages, Problems, and Solutions," *Biotechnology Advances* 37, no. 5 (2019): 746–770, https://doi.org/10.1016/j.biotechadv.2019.04.003.

16. X. Fan, S. Zhai, S. Xue, and L. Zhi, "Enzyme Immobilization Using Covalent Organic Frameworks: From Synthetic Strategy to COFs Functional Role," *ACS Applied Materials & Interfaces* 16, no. 31 (2024): 40371–40390, https://doi.org/10.1021/acsami.4c06556.

17. S. Qiao, H. Jin, A. Zuo, and Y. Chen, "Integration of Enzyme and Covalent Organic Frameworks: From Rational Design to Applications," *Accounts of Chemical Research* 57, no. 1 (2024): 93–105, https://doi.org/10.1021/acs.accounts.3c00565.

18. J. Zhang, Y. Li, J. Li, L. Zhu, and S. Jin, "Biomimetic Synthesis of Vesicular Covalent Organic Frameworks by Gemini Surfactants for In-Situ Enzyme Cascade Immobilization," *Nature Communications* 16, no. 1 (2025): 6046, https://doi.org/10.1038/s41467-025-60719-z.

19. C. G. Gruber, L. Frey, R. Guntermann, D. D. Medina, and E. Cortés, "Early Stages of Covalent Organic Framework Formation Imaged in Operando," *Nature* 630, no. 8018 (2024): 872–877, https://doi.org/10.1038/s41586-024-07483-0.

20. Z. F. Pang, S. Q. Xu, T. Y. Zhou, R. R. Liang, T. G. Zhan, and X. Zhao, "Construction of Covalent Organic Frameworks Bearing Three Different Kinds of Pores Through the Heterostructural Mixed Linker Strategy," *Journal of the American Chemical Society* 138, no. 14 (2016): 4710–4713, https://doi.org/10.1021/jacs.6b01244.

21. Y. Abiko, K. Onoue, Y. Yamamura, I. Nakazono, and T. Yoshida, "Studies on the Metabolism of Isonicotinic Acid Hydrazid in the Isolated Dog-Liver," *The Journal of Biochemistry* 48, no. 6 (1960): 838–845, https://doi.org/10.1093/oxfordjournals.jbchem.a127236.

22. T. Hatakeyama, H. Kohzaki, and N. Yamasaki, "A Microassay for Proteases Using Succinylcasein as a Substrate," *Analytical Biochemistry* 204, no. 1 (1992): 181–184, https://doi.org/10.1016/0003-2697(92)90158-4.

23. J. Phipps, L. Pinzon-Hererra, W. Fan, et al., "Insight Into Charged Drug Release From Metal–Organic Frameworks," *Nanoscale* 17, no. 27 (2025): 16523–16533, https://doi.org/10.1039/D5NR01357G.

24. J. Phipps, H. Chen, C. Donovan, et al., "Catalytic Activity, Stability, and Loading Trends of Alcohol Dehydrogenase Enzyme Encapsulated in a Metal–Organic Framework," *ACS Applied Materials & Interfaces* 12, no. 23 (2020): 26084–26094, https://doi.org/10.1021/acsami.0c06964.

25. W. Yang, W. Liang, L. A. O'Dell, et al., "Insights Into the Interaction Between Immobilized Biocatalysts and Metal–Organic Frameworks: A Case Study of PCN-333," *JACS Au* 1, no. 12 (2021): 2172–2181, https://doi.org/10.1021/jacsau.1c00226.

26. I. G. Kamphuis, K. H. Kalk, M. B. A. Swarte, and J. Drenth, "Structure of Papain Refined at 1.65 Å Resolution," *Journal of Molecular Biology* 179, no. 2 (1984): 233–256, https://doi.org/10.1016/0022-2836(84)90467-4.

27. K. Koupepidou, V. I. Nikolayenko, D. Sensharma, et al., "One Atom Can Make all the Difference: Gas-Induced Phase Transformations in Bisimidazole-Linked Diamondoid Coordination Networks," *Journal of the American Chemical Society* 145, no. 18 (2023): 10197–10207, https://doi.org/10.1021/jacs.3c01113.

28. F. Xie, L. Chen, E. M. Cedeño Morales, et al., "Complete Separation of Benzene-Cyclohexene-Cyclohexane Mixtures via Temperature-Dependent Molecular Sieving by a Flexible Chain-Like Coordination Polymer," *Nature Communications* 15, no. 1 (2024): 2240, https://doi.org/10.1038/s41467-024-46556-6.

29. L. Feng, K. Y. Wang, X. L. Lv, T. H. Yan, and H. C. Zhou, "Hierarchically Porous Metal–Organic Frameworks: Synthetic Strategies And Applications," *National Science Review* 7, no. 11 (2020): 1743–1758, https://doi.org/10.1093/nsr/nwz170.

30. J. Liang, J. Ruan, B. Njegic, et al., "Insight Into Bioactivity of In-Situ Trapped Enzyme-Covalent-Organic Frameworks," *Angewandte Chemie International Edition* 62, no. 23 (2023): 202303001, https://doi.org/10.1002/anie.202303001.

31. F. Li and Z. Zhou, "Micro/Nanostructured Materials for Sodium Ion Batteries and Capacitors," *Small* 14, no. 6 (2018): 1702961, https://doi.org/10.1002/smll.201702961.

32. Y. Song and S. Ma, "Pore Engineering In Metal–Organic Frameworks And Covalent Organic Frameworks: Strategies And Applications," *Chemical Science* 16, no. 26 (2025): 11740–11767, https://doi.org/10.1039/D5SC01635E.

Supporting Information

Additional supporting information can be found online in the Supporting Information section.

Supporting File: smll75016-sup-0001-SuppMat.docx.